

The Intricate Structural Chemistry of $M^{II}_{2n}L_n$ -Type Assemblies

Giacomo Cecot,[†] Mathieu Marmier,[†] Silvano Geremia,[§] Rita De Zorzi,[§] Anna V. Vologzhanina,[‡] Philip Pattison,^{#,‡} Euro Solari,[†] Farzaneh Fadaei Tirani,[†] Rosario Scopelliti,[†] and Kay Severin^{*,†}

[†]Institute of Chemical Sciences and Engineering, École Polytechnique Fédérale de Lausanne (EPFL), CH-1015 Lausanne, Switzerland

[§]Centro di Eccellenza in Biocristallografia, Dipartimento di Scienze Chimiche e Farmaceutiche, Università di Trieste, Italy

[‡]Nesmeyanov Institute of Organoelement Compounds of the Russian Academy of Sciences, 119991 Moscow, Russia

[#]Institute of Physics, Ecole Polytechnique Fédérale de Lausanne (EPFL), 1015 Lausanne, Switzerland

[‡]Swiss-Norwegian Beamline, ESRF, Grenoble, France.

ABSTRACT: The reaction of *cis*-blocked, square planar M^{II} complexes with tetrapotic N-donor ligands is known to give metallasupramolecular assemblies of the formula $M_{2n}L_n$. These assemblies typically adopt barrel-like structures, with the ligands paneling the sides of the barrels. However, alternative structures are possible, as demonstrated by the recent discovery of a Pt_8L_4 cage with unusual gyrobifastigium-like geometry. To date, the factors which govern the assembly of $M^{II}_{2n}L_n$ complexes are not well understood. Herein, we provide a geometric analysis of $M_{2n}L_n$ complexes, and we discuss how size and geometry of the ligand is expected to influence the self-assembly process. The theoretical analysis is complemented by experimental studies using different *cis*-blocked Pt^{II} complexes and metalloligands with four divergent pyridyl groups. Mononuclear metalloligands gave mainly assemblies of type Pt_8L_4 , which adopt barrel- or gyrobifastigium-like structures. Larger assemblies can also form, as evidenced by the crystallographic characterization of a $Pt_{10}L_5$ complex and a $Pt_{16}L_8$ complex. The former adopts a pentagonal barrel structure, whereas the latter displays a barrel structure with a distorted square orthobicupola geometry. The $Pt_{16}L_8$ complex has a molecular weight of more than 23 kDa and a diameter of 4.5 nm, making it the largest, structurally characterized $M_{2n}L_n$ complex described to date. A dinuclear metalloligand was employed for the targeted synthesis of pentagonal $Pt_{10}L_5$ barrels, which are formed in nearly quantitative yields.

INTRODUCTION

The chemistry of coordination cages has advanced dramatically in recent years. Thanks to this progress, it is now possible to prepare cages with diverse geometries and functions.¹ In contrast to coordination cages with enclosed cavities, there are fewer examples of metallasupramolecular structures with barrel-like structures, and applications of such barrels are largely unexplored.²⁻⁷ In view of the fact that purely organic barrels have been used extensively in the area of molecular transport and sensing,⁸ one can expect to find interesting functions for metal-based barrels as well. To further advance this field, a better understanding of the factors which control the assembly of coordination barrels is of importance. Furthermore, an extension of the available structure types is of interest.

The combination of *cis*-blocked Pd^{II} or Pt^{II} complexes having two available coordination sites with tetrapotic N-donor ligands is arguably the most explored synthetic strategy for the formation of coordination barrels.²⁻⁵ For ligands which can adopt a concave geometry (the coordinate vectors all point towards one side), the formation of small M_4L_2 complexes is possible (Figure 1, **A**).² However, the utilization of ligands with a ‘flat’ backbone is more common (the coordinate vectors are all in the same plane). For such ligands, the resulting barrels have mostly trigonal prismatic M_6L_3 structures (Figure 1, **B**)³ or tetragonal prismatic M_8L_4 structures (Figure 1, **C**).⁴ To the best of our knowledge, only one example of an $M_{2n}L_n$ -type barrel with more than eight metal centers has been described, and that is a

hexagonal $Pt_{12}L_6$ complex which was reported by the group of Mukherjee in 2008 (Figure 1, **E**).⁵ This complex was obtained by combination of a tetrapyrrolyl-porphyrin ligand and $(dppf)Pt(OTf)_2$ ($dppf$ = bis(diphenylphosphino)ferrocene).

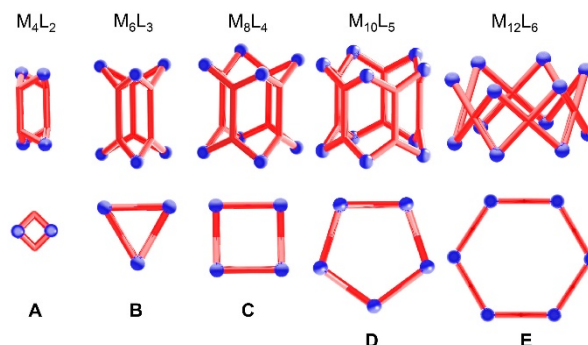


Figure 1. $M^{II}_{2n}L_n$ assemblies can adopt barrel-like structures. Examples of structures **A**, **B**, **C**, and **E** have been reported previously.

We have recently reported the synthesis of novel M_8L_4 complexes, which were prepared by combination of $[Ph_2P(CH_2)_nPPh_2]M(OTf)_2$ ($M = Pd, Pt$) with tetrapotic metalloligands.⁹ These complexes were found to adopt an unusual gyrobifastigium-like geometry.¹⁰ This unexpected finding made us realize that the factors which govern the self-assembly of $M_{2n}L_n$ complexes are not well understood. Attempts to provide

a better understanding of the intricate structural chemistry of $M_{2n}L_n$ assemblies are described below.

RESULTS AND DISCUSSION

Geometrical considerations. Coordination-based self-assembly relies on geometric considerations as a prognostic tool. Knowing the preferred geometry of metal complexes and the coordinate vectors of the ligand allows making predictions about the structure of the metallasupramolecular assembly. Unfortunately (or luckily, depending on the viewpoint), there is still ample room for serendipity and surprises, because the thermodynamic stability of a metallasupramolecular assembly is influenced by multiple parameters, some of which are independent from geometry (e.g. solvent or counter ions). Nevertheless, a geometric analysis can serve as a useful guideline.

Let's consider $M_{2n}L_n$ complexes based on 'flat', tetatopic ligands with D_{2h} or D_{4h} symmetry. Ligands of this kind can form barrel structures with $n \geq 3$. The barrels can be described as prisms with an n -sided polygonal base and n faces, which are paneled by the ligands. The faces cross at an angle γ , with γ being defined by n (for $n = 3$, we observe a trigonal prism with $\gamma = 60^\circ$; for $n = 4$, we observe a tetragonal prism with $\gamma = 90^\circ$, etc.). The geometry of the ligand is defined by the angle α of the two coordinate vectors, which point to two adjacent metal centres on the n -sided polygonal base (Figure 2). The geometry of the metal complex, on the other hand, is defined by the coordination angle β . The three angles are related by the equation: $\sin(\alpha/2) = \sin(\beta/2) \cdot \sin(\gamma/2)$ (for a derivation see the Supporting Information, SI).

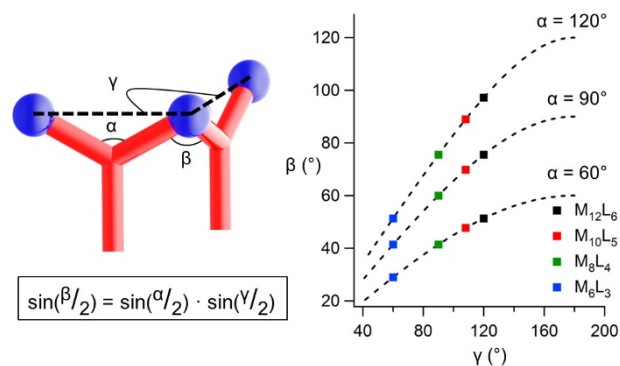


Figure 2. Geometric analysis of $M_{2n}L_n$ complexes with a prismatic structure. The graph depicts the correlation between the angle α , defining the orientation of the coordinate vectors of the ligand, the angle β , defining the coordination geometry of the metal, and the angle γ , which is given by the aggregation number n .

Figure 2 gives the relationship between the angles β and γ for prismatic barrels with $n = 3-6$. $M_{2n}L_n$ -type assemblies are often formed with cis-blocked Pd^{II} or Pt^{II} complexes. These square planar metal complexes have a preferred coordination angle of $\beta \sim 90^\circ$. If the coordinate vectors of the ligand form an angle of $\alpha = 120^\circ$, then a nearly 'perfect' coordination angle of $\beta = 89^\circ$ would be observed for a pentagonal prism with $n = 5$. For a tetragonal prism with $n = 4$, the coordination angle would be reduced to $\beta = 76^\circ$, and a trigonal prism would show a coordination angle of only $\beta = 51^\circ$. It can be concluded that for a perfectly rigid ligand with $\alpha = 120^\circ$, the formation of entropically

favoured small prisms with $n = 3$ or 4 would lead to a constrained geometry at the metal.

A rectangular, D_{2h} symmetric ligand with $\alpha = 120^\circ$ has the possibility to coordinate in a different orientation, such that the coordinate vectors form an angle of 60° instead of 120° . Figure 3 shows the two possible isomers **C** and **C'** for a tetragonal prism with $n = 4$. The formation of isomer **C'** would lead to a very strained geometry at the metal with $\beta = 41^\circ$. Increasing the aggregation number n does not improve the situation substantially, because even for a hexameric barrel with $n = 6$, the coordination angle β is still only 51° . It is worth pointing out that the formation of isomers such as **C'** has been discussed in the literature,^{4c} but for all crystallographically characterized $M_{2n}L_n$ barrels based on rectangular ligands, it is the larger angle α which points to the n -sided polygonal base.²⁻⁵

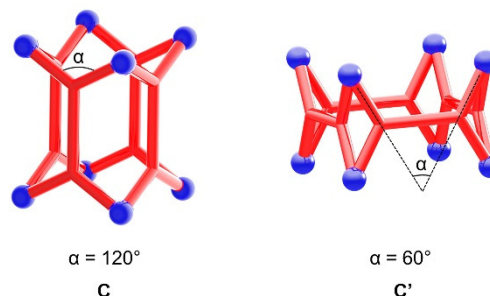


Figure 3. Hypothetical isomers **C** and **C'** for M_3L_4 complexes based on a tetatopic ligand. The coordinate vectors of two adjacent donor atoms of the ligand cross at angles of $\alpha = 120^\circ$ or 60° , respectively.

For our geometric analysis, we have assumed that the ligand is perfectly rigid. However, real ligands always have some degree of conformational flexibility. Furthermore, it is possible that the coordinate vectors of the ligand are not perfectly aligned with the metal-ligand bonds. This flexibility is expected to favor the formation of smaller assemblies. Reviewing the available experimental data shows that a preference for complexes with a small aggregation number n can indeed be observed.

Figure 4 lists some of the tetatopic N-donor ligand, which have been used for the construction of $M^{II}_{2n}L_n$ barrels. Ligand **L1** has a rather large angle α between the coordinate vectors of around 141° . If we assume a perfectly rigid ligand, we can calculate the hypothetical coordination angles β for prismatic $M_{2n}L_n$ assemblies. The best match for assemblies based on square planar M^{II} complexes is found for $n = 4$ with $\beta = 84^\circ$, which is close to the ideal value of $\beta = 90^\circ$. Experimentally, ligand **L1** was found to make a trigonal prismatic assembly ($n = 3$) when combined with $(Et_3P)_2Pt(OTf)_2$.^{3b} The observed N-Pt-N angles are $\beta = 82^\circ$ on average, which is much larger than the calculated angle of $\beta = 56^\circ$ for an assembly with $n = 3$. The deviation is the result of a significant distortion of the ligand. Apparently, the entropic advantage of forming a smaller assembly compensates the enthalpy penalty, which is associated with ligand distortion. As we will see for the examples discussed below, the formation of smaller assemblies along with ligand distortion is a common phenomenon.

The tetrapyrrolyl ligands **L2-L4** all have coordinate vectors with angles of 120° . As outlined in Figure 2, such ligands are expected to form pentagonal barrels ($n = 5$) if ligand distortion is not an option. Experimentally, it was found that **L2** and **L4** form

trigonal prismatic assemblies ($n = 3$), and **L3** gave rise to a tetrameric barrel ($n = 4$).^{3a,c} The difference can be explained by the presence of alkynyl spacers in **L2** and **L4**, which increase the flexibility of the ligand.¹¹ However, steric effects might also play a role as discussed in more detail below.

Ligand **L5** is relatively rigid, and it features coordinate vectors with angles of only 105° . When combined with $(\text{dppf})\text{M}(\text{OTf})_2$ complexes, tetrameric barrels were observed.^{4c} Unfortunately, crystallographic data are not available, and ligand distortion and coordination angles cannot be evaluated. It is clear, however, that the small angle of $\alpha = 105^\circ$ will lead to a strained geometry for a tetrameric assembly.

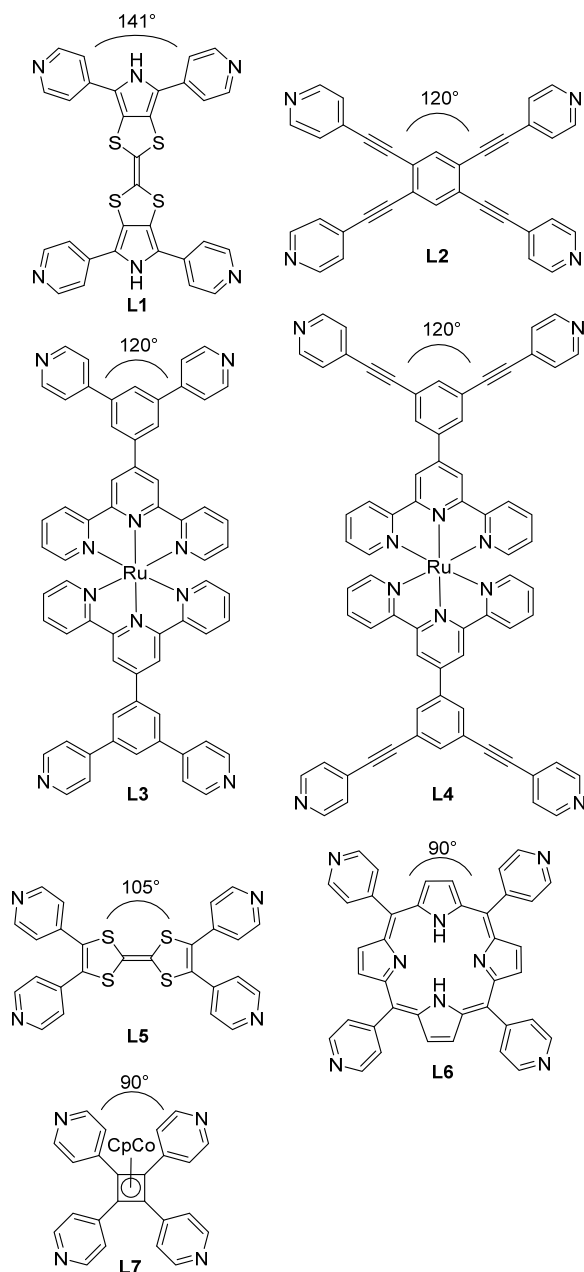


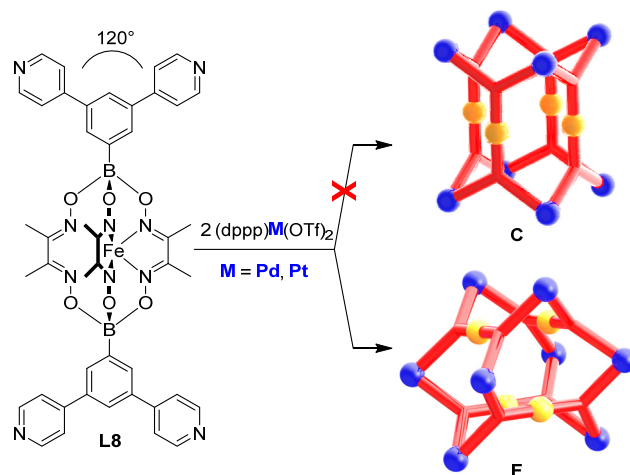
Figure 4. Tetrapic pyridyl ligands which have been employed before for the synthesis of prismatic $\text{M}^{\text{II}}_2\text{L}_n$ complexes (refs. 3a, 3b, 3c, 4c, 5, 12).

The tetra(4-pyridyl)porphyrin ligand **L6** stands out because it forms a hexameric barrel ($n = 6$) when combined with

$(\text{dppf})\text{Pt}(\text{OTf})_2$.⁵ The formation of a large assembly can be rationalized with the help of our geometric analysis. As shown in Figure 2, ligands with an angle of $\alpha = 90^\circ$ will favor high aggregation numbers, because low aggregation numbers would result in very small coordination angles at the metal. For a hexameric barrel, one would expect a coordination angle of $\beta = 76^\circ$. The experimentally observed N-Pt-N angles are 80° on average, indicating some ligand distortion.

The organometallic pyridyl ligand **L7** features a Co^{I} sandwich complex at its core. Similar to ligand **L6**, the coordinate vectors cross at an angle of $\alpha = 90^\circ$. The combination of **L7** with $(\text{en})\text{Pd}(\text{NO}_3)_2$ (en = ethylenediamine) was found to give an assembly of formula $[(\text{en})\text{Pd}]_{12}(\text{L7})_6(\text{NO}_3)_{24}$, as evidenced by mass spectrometry.¹² The authors of this study proposed a cubic structure with the ligands panelling the six faces. Such an arrangement would lead to ‘ideal’ N-Pd-N angles of 90° . However, the formation of a hexameric barrel, as observed for ligand **L6**, cannot be excluded based on the available analytical data. Ligand **L7** was also combined with $(\text{Me}_3\text{P})_2\text{Pt}(\text{OTf})_2$. The reaction product was proposed to have a trigonal prismatic structure ($n = 3$),^{3c} even though the mass spectrum showed a peak which could be assigned to an assembly with $n = 6$. The MS data was rationalized by assuming the aggregation of two trigonal prisms via weak electrostatic forces. A cubic or a hexagonal barrel structure was excluded based on the results of DOSY measurements, which were not in line with the expected size of an assembly with $n = 6$. From a purely geometrical point of view, the formation of a trigonal prism is surprising, because a ligand with $\alpha = 90^\circ$ would lead to an assembly with a *very* small coordination angle at the metal center ($\beta = 45^\circ$ for a rigid ligand).

We have recently described the synthesis of the metalloligand **L8** (Scheme 1).⁹ Combination of this ligand with $(\text{dppp})\text{M}(\text{OTf})_2$ complexes ($\text{M} = \text{Pd}, \text{Pt}$; dppp = 1,3-bis(diphenylphosphino)propane) resulted in the formation of assemblies of the formula $[(\text{dppp})\text{M}]_8(\text{L8})_4(\text{OTf})_{16}$, as evidenced by mass spectrometry. The result of a crystallographic analysis of the Pd complex gave a surprising result: instead of the expected barrel structure of type C, we observed the formation of an unprecedented gyrobifastigium-like structure (**F**).⁹



Scheme 1. Synthesis of Assemblies with a Gyrobifastigium-like Structure **F**.

The clean formation of a gyrobifastigium-like structure was unexpected, in particular since the closely related metalloligand **L3** was found to give a tetrameric barrel of type C with the same

(dppp)Pd(OTf)₂ complex. It is worth noting that similar N-Pd-N angles were observed for the tetragonal barrel based on ligand **L3** (N-Pd-N_{av.} = 84.8°) and for the gyrobifastigium based on **L8** (N-Pd-N_{av.} = 84.3°). Reduced steric constraints at the metal center were thus not the driving force behind the formation of structure **F**.

Steric interactions between the ligand cores should be considered as a potential factor influencing the stability of such assemblies. In fact, Beves et al. have argued that favorable π - π stacking interactions between the Ru(tpy)₂ units are found for the tetrameric barrel based on ligand **L3**.^{3a} In the case of ligand **L8**, steric interactions between the central Fe^{II} clathrochelate complexes are expected to be unfavorable,¹³ at least in solvents where solvophobic effects can be neglected.¹⁴

Figure 5 shows a comparison of the distances between the ligand cores for structures of type **C**, **F**, and **D**. The geometry of the gyrobifastigium-like cage **F** depends on the dimensions of the ligand. For the analysis, we have assumed that the ligand panels a rectangle whose edges **x** and **y** are correlated by the equation $x = 2^{1/2} y$ (as found approximately for ligand **L8**). For a tetrameric barrel, the ligand centers are arranged in form of a square with the edge lengths **a**. In the case of isomer **F**, the ligand centers are arranged in the form of a distorted tetrahedron, showing two short edges **a** and four long edges **b**. One can calculate that **b** is 22% longer than **a**. In other words, the formation of a gyrobifastigium-like structure leads to reduced steric interactions between the central parts of the ligands. For ligands with bulky cores such as **L8**, isomer **F** could thus be favored over isomer **C**.

A different possibility to increase the distances between the central parts of the ligand is the formation of aggregates with a high association number *n*. In a pentagonal barrel of type **D**, for example, the distance between the ligand centers is increased by 14% with respect to tetragonal barrel of type **C** (Figure 5).

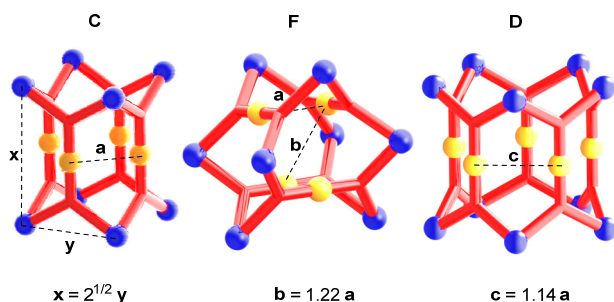


Figure 5. Increased distances between the ligand cores (indicated by orange spheres) are observed for the gyrobifastigium-like structure **F** and the pentagonal barrel **D**, when compared to the tetragonal barrel **C**.

As mentioned above, the ligand dimensions are of importance for the geometry of gyrobifastigium-like assemblies. If the length of the ligand is increased with respect to its width, the cage will ‘flatten’. This effect is shown in Figure 6, which depicts two gyrobifastigium-like assemblies based on *D*_{2h} symmetric ligands with a different aspect ratio. The angle δ , which is defined by the planes of two adjacent ligands, will become larger if the aspect ratio of the ligand increases. At the same time, the distance **b** between opposite ligand centers will shrink. For ligands approaching an aspect ratio of $x = 2y$, the formation of a gyrobifastigium-like structure will become impossible. For the other extreme, a square ligand with $x = y$, the angle δ would

be reduced to 60°, resulting in very small coordination angle at the corresponding metal center. It can be concluded that the geometric requirements for forming a non-strained gyrobifastigium-like structure of type **F** are rather strict, and only few ligands have the potential to do so. It is therefore not surprising that structures of type **F** have not been reported more frequently.

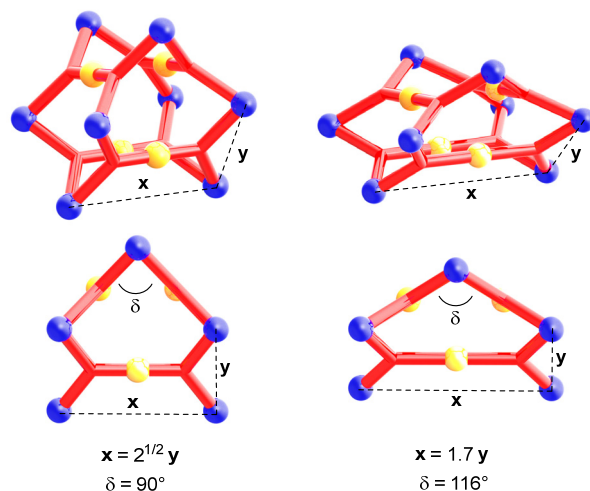


Figure 6. Geometry of gyrobifastigium-like structures based on ligands with a different aspect ratio.

M_{2n}L_n complexes based on mononuclear metalloligands:

For our new experimental work, we have used the metalloligands **L9–L12** (Figure 7). All these ligands all feature terminal di(pyridine-4-yl)phenyl groups, which are attached to boronate-ester-capped clathrochelate complexes.

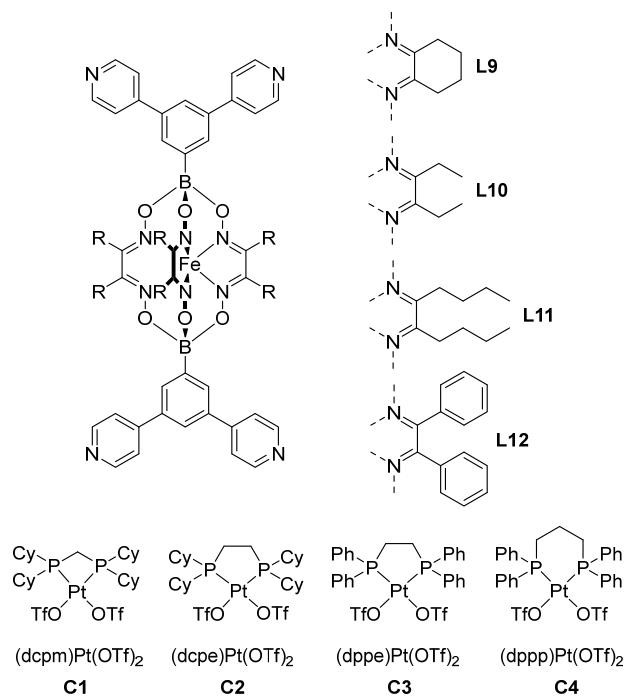


Figure 7. Structures of the metalloligands **L9–L12** and of the Pt complexes **C1–C4** used in the current work.

The synthesis of **L10** has been described previously.⁹ It can be obtained by a four-fold cross-coupling reaction of a clathrochelate complex with terminal 3,5-dibromophenyl groups and 4-pyridylboronic acid. The new ligands **L9**, **L11**, and **L12** were prepared accordingly (for details see SI).

The central clathrochelate complexes of the metalloligands **L9**–**L12** have side chains, which differ in terms of size and flexibility. The difference is evident when comparing the solid state structures of the ligands, which were determined by X-ray diffraction. Figure 8 depicts space-filling representations of the clathrochelate cores of **L9**, **L11**, and **L12**, with view along the B···B axis. The cyclohexyl side chains of **L9** and the phenyl side chains of **L12** display limited conformational flexibility. As a result, we observe complexes with approximate C_3 symmetry. The butyl side chains of **L1** are more flexible, and a reduced symmetry is observed. It is also evident that the ligands **L11** and **L12** are overall thicker than ligand **L9**.

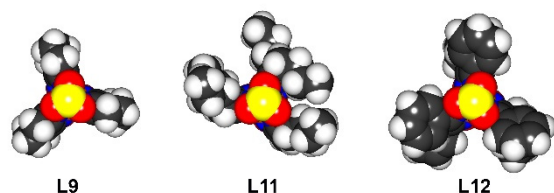


Figure 8. Space filling representation of the molecular structures of **L9**, **L11**, and **L12** in the crystal. The terminal di(pyridine-4-yl)phenyl groups have been omitted to facilitate a comparison of the central clathrochelate cores. Color coding: C: gray, B: yellow, Fe: orange, N: blue, O: red, H: light gray.

$M_{2n}L_n$ -type assemblies were formed by combining the metalloligands **L9**–**L12** with the *cis*-blocked Pt^{II} complexes **C1**–**C4** (Figure 7). The reactions were performed in acetonitrile using an **L**:**C** ratio of 1:2.1 and a concentration of [**L**] \sim 1.3 mM. Equilibration was ensured by tempering the reaction mixtures at 50 °C for 24 h (NMR measurements of reactions performed in CD_3CN confirmed that there are no further changes after 24 h). The reaction products were then precipitated by addition of diethyl ether or diethyl ether/pentane (1:4). After isolation and drying under vacuum, the products were re-dissolved in CD_3CN (\sim 2 mg/mL). As primary analyses tools, we have employed ^{31}P NMR spectroscopy and high resolution ESI mass spectrometry. The ^{31}P NMR spectra were used to determine whether the self-assembly process gave rise to a defined product. If one product was formed in yields higher than 85% (the yield was approximated by integration of the ^{31}P NMR signals), the reaction was classified as ‘clean’ (Table 1). Otherwise, the outcome of the reaction was labelled as a ‘mixture’. It is worth noting that the barrel structures **A**–**E** (Figure 1) should all give only one signal in the ^{31}P NMR spectra (along with the ^{195}Pt satellites). For the gyrobifastigium-like structure **F** (Figure 5), on the other hand, one expects two signals of equal intensity, because there are two types of Pt corners in the structure. For spectra with two equally intense signals, we have assumed that they belong to a gyrobifastigium-like structure.

Table 1 summarizes the NMR and MS analyses for 15 reaction mixtures (the combination of **L12** with **C4** resulted in the formation of a precipitate, and was not included). The dominant $Pt_{2n}L_n$ species detected by MS was always a Pt_8L_4 complex. According to ^{31}P NMR spectroscopy, most of them appear to be gyrobifastigium-like structures (two equally intense singlets). ESI high-resolution mass spectrometry enabled us to detect small peaks, which can be attributed to larger $Pt_{10}L_5$, $Pt_{16}L_8$, and

$Pt_{24}L_{12}$ assemblies. In view of the crystallography results described below, we assume that these complexes are present in small amounts in the reaction mixture and not formed during the MS experiment. It should be noted that we have not been able to assign all peaks in the MS spectra. As a consequence, it is possible that we observed a ‘mixture’ by ^{31}P NMR spectroscopy, but only Pt_8L_4 complex by mass spectrometry (e.g. for the combination of **L9** and **C2**).

Table 1. Analysis of Different **L/C** Combinations by ESI Mass Spectrometry and ^{31}P NMR Spectroscopy.^a

ligand	complex	MS _{major}	MS _{minor}	^{31}P NMR ^b
L9	C1	Pt_8L_4	$Pt_{16}L_8$	mixture
	C2	Pt_8L_4	/	mixture
	C3	Pt_8L_4	$Pt_{16}L_8$	clean ^c
	C4	Pt_8L_4	$Pt_{16}L_8$	clean ^c
L10	C1	Pt_8L_4	$Pt_{10}L_5$, $Pt_{16}L_8$	clean ^c
	C2	Pt_8L_4	/	mixture
	C3	Pt_8L_4	$Pt_{16}L_8$	clean ^c
	C4	Pt_8L_4	$Pt_{10}L_5$, $Pt_{16}L_8$	clean ^c
L11	C1	Pt_8L_4	$Pt_{16}L_8$	clean ^c
	C2	Pt_8L_4	$Pt_{16}L_8$	clean ^c
	C3	Pt_8L_4	$Pt_{16}L_8$	clean ^c
	C4	Pt_8L_4	$Pt_{16}L_8$, $Pt_{24}L_{12}$	clean ^c
L12	C1	Pt_8L_4	$Pt_{16}L_8$	clean ^d
	C2	Pt_8L_4	/	mixture
	C3	Pt_8L_4	$Pt_{10}L_5$	mixture

^a The reactions between the ligands and the metal complexes were performed as described in the main text. ^b If the NMR data indicate the presence of one main species with an estimated yield of higher than 85%, the reaction outcome is labelled as ‘clean’. Otherwise, it is labelled as a ‘mixture’. It should be noted that spectra of ‘clean’ reactions may show small peaks due to minor amounts of side products. ^c Two equally intense signals, indicating a gyrobifastigium-like structure. ^d One signal, indicating a barrel structure.

A representative mass spectrum is shown in Figure 9. The spectrum was obtained for the product of the reaction between ligand **L11** and complex **C4**. Dominant peaks can be assigned to an assembly with the formula $[(dppp)Pt]_8(L11)_4(OTf)_n$. In addition, there are significant peaks for a $[(dppp)Pt]_{16}(L11)_8(OTf)_n$ complex, and a very small peak which could be attributed to a $[(dppp)Pt]_{24}(L11)_{12}(OTf)_{39}$ complex.

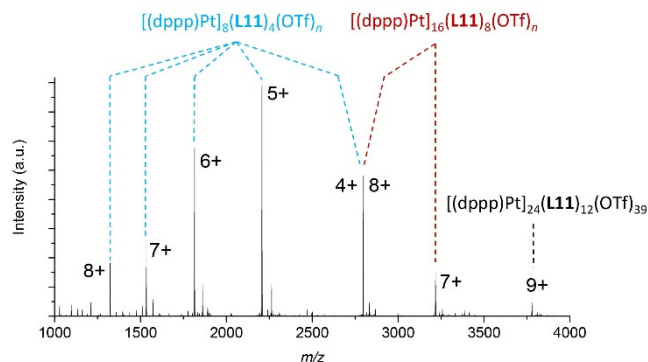


Figure 9. ESI MS analysis of the reaction between ligand **L11** and complex **C4**.

In addition to the solution-based analyses, we have carried out X-ray diffraction analyses of seven different $M_{2n}L_n$ complexes. Single crystals of the assemblies were obtained by slow diffusion of diethyl ether into solution of the complexes in acetonitrile. Due to the complexity of the structures, the crystallographic analyses were challenging, even though we had access to a synchrotron beamline. Problems encountered include the presence of co-crystallized, disordered solvent molecules, disordered triflate anions, disordered clathrochelate side chains, and non-merohedral twinning for crystals of complex **C1** with ligand **L10** (for details see SI). Despite these problems, it was possible to establish the connectivity of the complexes with good precision.

An overview of the results is given in Figure 10. For two combinations (**L9** + **C2** and **L12** + **C1**), we were able to crystallize tetragonal barrel structures. Gyrobifastigium-like structures were observed for three reaction mixtures, all of which involve the platinum complex **C4**. Crystals of a pentagonal barrel were obtained from the reaction between **L10** and **C1**, and a large $Pt_{16}L_8$ complex was observed for the reaction between **L11** and **C3**. A more detailed discussion of these structures is given below.

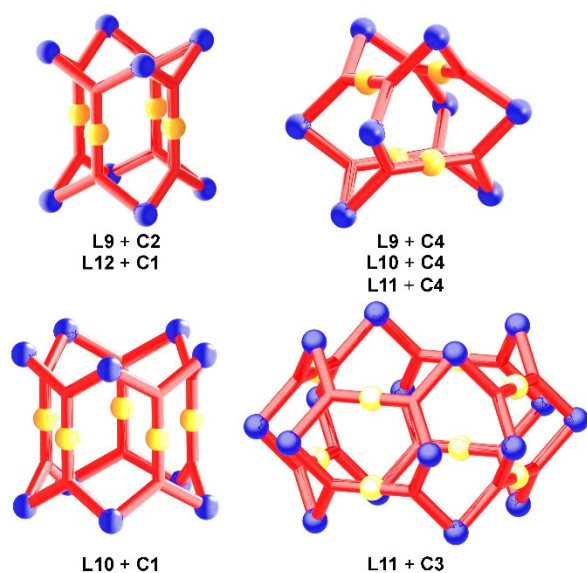


Figure 10. Schematic representation of the $M_{2n}L_n$ assemblies, which were characterized by single crystal X-ray diffraction. The corresponding building blocks are given below the graphics.

In our first communication, we have argued that the gyrobifastigium geometry is favored over a tetragonal barrel structure because the former displays reduced steric interactions between the clathrochelate cores of the metalloligands.⁹ The crystallization of the complexes $[(dcpe)Pt]_8(L9)_4(OTf)_{16}$ (Figure 11) and $[(dcpe)Pt]_8(L12)_4(OTf)_{16}$ (Figure 12) is evidence that tetragonal barrel structures are possible, even when using these bulky metalloligands. However, it is worth noting that one can observe a sterically congested barrel interior, in particular for the tetragonal barrel based on ligand **L12** (Figure 12, c). Twelve out of the 18 phenyl side chains of the clathrochelate complexes pack closely against each other. For the barrel based on ligand **L9**, one can also observe tight, interdigitating cyclohexyl side chains (Figure 11, c), but the steric congestion is less pronounced.

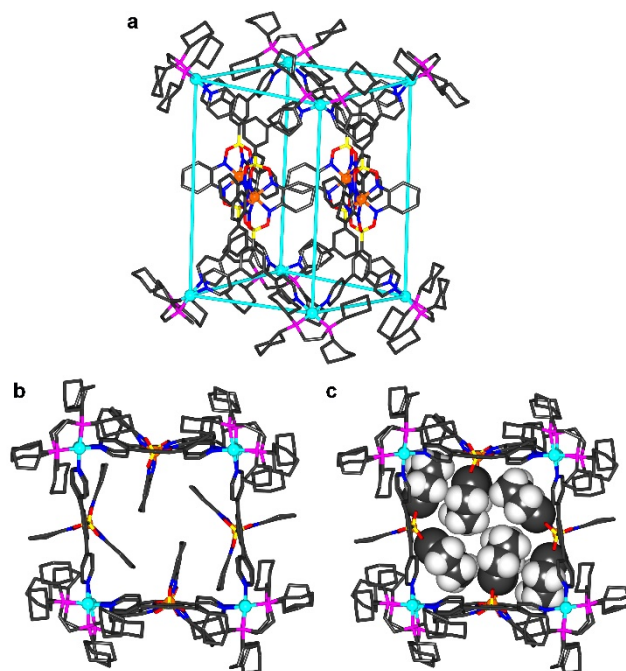


Figure 11. Molecular structure of complex $[(dcpe)Pt]_8(L9)_4(OTf)_{16}$ in the crystal with view from the side (a) and along the barrel axis (b and c). The barrel geometry is indicated by (virtual) Pt-Pt bonds. In view c, the cyclohexyl side chains, which point to the interior of the barrel, are shown with a space-filling representation. Color coding: C: gray, B: yellow, Fe: orange, Pt: cyan, P: purple, N: blue, O: red, H: light gray. Most hydrogen atoms, all counter ions and solvent molecules are omitted for clarity.

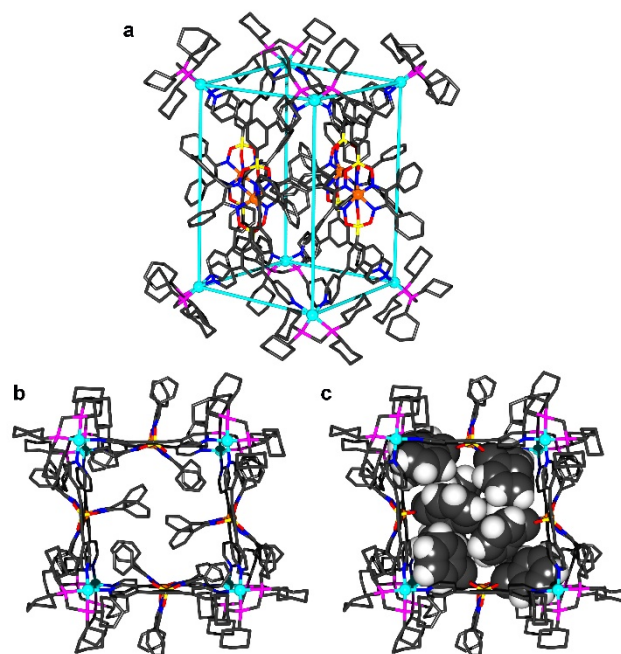


Figure 12. Molecular structure of complex $[(dcpm)Pt]_8(L12)_4(OTf)_{16}$ in the crystal with view from the side (a) and along the barrel axis (b and c). The barrel geometry is indicated by (virtual) Pt-Pt bonds. In view c, the phenyl side chains, which point to the interior of the barrel, are shown with a space-filling representation. Color coding: C: gray, B: yellow, Fe: orange, Pt: cyan, P: purple, N: blue, O: red, H: light gray. Most hydrogen atoms, all counter ions and solvent molecules are omitted for clarity.

It is interesting to compare the structural results with the solution-based analysis. For the combination of **L12** and **C1**, the reaction was found to be ‘clean’, with a main product featuring one signal in the ^{31}P NMR spectrum (Table 1). It is likely that the tetragonal barrel observed by X-ray crystallography is also the dominant species in solution. The clean formation of a tetragonal barrel is intriguing, because gyrobifastigium-like structures seem to be favored for most L/C combinations (Table 1). One possible explanation is that π - π interactions between the tightly packed phenyl chains stabilize the barrel arrangement. For the combination of **L9** and **C2**, we observed a mixture of products by ^{31}P NMR spectroscopy, and the tetragonal barrel is not particularly favored.

For reactions of the platinum complex **C4** with the ligands **L9**, **L10**, and **L11**, we were able to obtain crystals of complexes with a gyrobifastigium-like geometry (Figure 13). The three structures are overall very similar. The four quadrilateral faces of the polyhedron are paneled by the tetratopic metalloligands, whereas the four triangular faces are open. The distortion with respect to a perfect gyrobifastigium geometry comes from the fact that the quadrilateral faces are not square, as expected for a regular gyrobifastigium, but rectangular. Still, the D_{2d} symmetry of a gyrobifastigium is approximately conserved. The structures observed by X-ray crystallography also seem to be the dominant species in solution, as indicated by the MS and ^{31}P NMR data (Table 1).

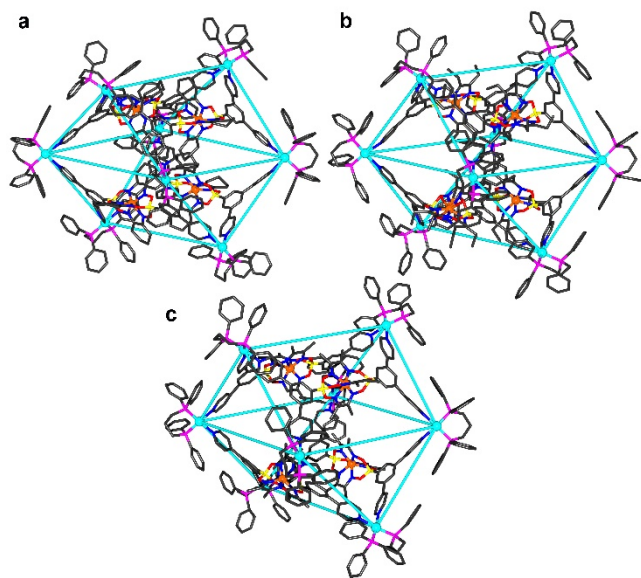


Figure 13. Molecular structures of the complexes $[(\text{dppp})\text{Pt}]_8(\text{L9})_4(\text{OTf})_{16}$ (a), $[(\text{dppp})\text{Pt}]_8(\text{L10})_4(\text{OTf})_{16}$ (b), and $[(\text{dppp})\text{Pt}]_8(\text{L11})_4(\text{OTf})_{16}$ (c) in the crystal. The gyrobifastigium-like geometry is indicated by (virtual) Pt-Pt bonds. Color coding: C: gray, B: yellow, Fe: orange, Pt: cyan, P: purple, N: blue, O: red. Hydrogen atoms, counter ions and solvent molecules are omitted for clarity. The butyl side chains of $[(\text{dppp})\text{Pt}]_8(\text{L11})_4(\text{OTf})_{16}$ are highly disordered, and only the first carbon atoms could be identified in the electron density map.

Pentagonal prismatic M_{10}L_5 structures (Figure 1, D) have not been described before, and we were thus intrigued by the structural characterization of complex $[(\text{dcpm})\text{Pt}]_{10}(\text{L10})_5(\text{OTf})_{20}$ (Figure 14). The barrel interior is partially filled with 10 ethyl side chains, some of which are in close contact to each other. The ESI mass spectrum of the **C1/L10** mixture indicates that

$[(\text{dcpm})\text{Pt}]_{10}(\text{L10})_5(\text{OTf})_{20}$ is also present in solution. The dominant product for this combination of building blocks is a $[(\text{dcpm})\text{Pt}]_8(\text{L10})_4(\text{OTf})_{16}$ complex with a gyrobifastigium-like geometry, as evidenced by ^{31}P NMR spectroscopy and mass spectrometry (Table 1).

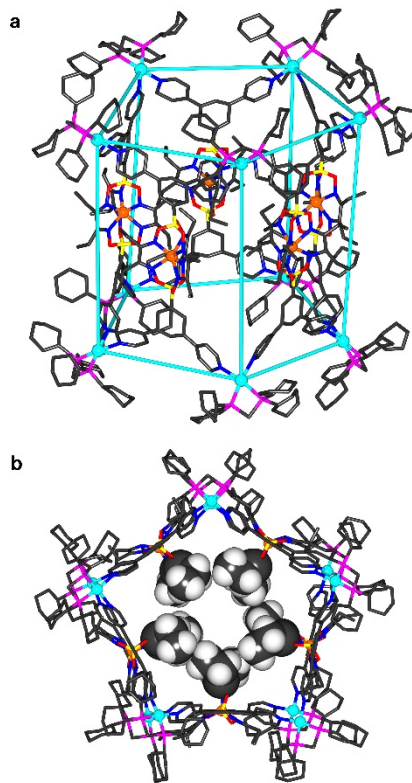


Figure 14. Molecular structure of complex $[(\text{dcpm})\text{Pt}]_{10}(\text{L10})_5(\text{OTf})_{20}$ in the crystal with view from the side (a) and along the barrel axis (b). The barrel geometry is indicated by (virtual) Pt-Pt bonds. In view b, the ethyl side chains, which point to the interior of the barrel, are shown with a space-filling representation. Color coding: C: gray, B: yellow, Fe: orange, Pt: cyan, P: purple, N: blue, O: red, H: light gray. Most of the hydrogen atoms and all counter ions are omitted for clarity.

As indicated in Table 1, we have been able to detect for several L/C combinations small peaks in the MS spectra, which can be assigned to Pt_{16}L_8 complexes. For the reaction of **C3** with **L11**, we could characterize such an assembly by single crystal X-ray diffraction. The $[(\text{dppe})\text{Pt}]_{16}(\text{L11})_8(\text{OTf})_{32}$ complex displays a unique geometry. The Pt atoms are arranged in the form of a distorted square orthobicupola structure (Figure 15). The square orthobicupola belongs to the family of Johnson polyhedra (J28).¹⁵ It is formed from 10 squares and 8 equilateral triangles. In our case, 8 of the 10 rectangular faces are paneled by the tetratopic ligands. The two open rectangular faces are positioned opposite to each other. As a result, the complex displays a barrel-like structure. The size and the weight of the complex are noteworthy. The polycationic part of the complex is composed of 1112 non-hydrogen atoms, and it has a molecular weight of 23 kDa. To put this value into perspective: the protein myoglobin has a molecular weight of only 17 kDa.¹⁶ The diameter of the barrel, as defined by the maximum C···C distance, is 4.5 nm. For comparison: the largest $\text{M}_{2n}^{\text{II}}\text{L}_n$ complex described

so far, the hexagonal barrel of Mukherjee, has a diameter of 2.7 nm.⁵

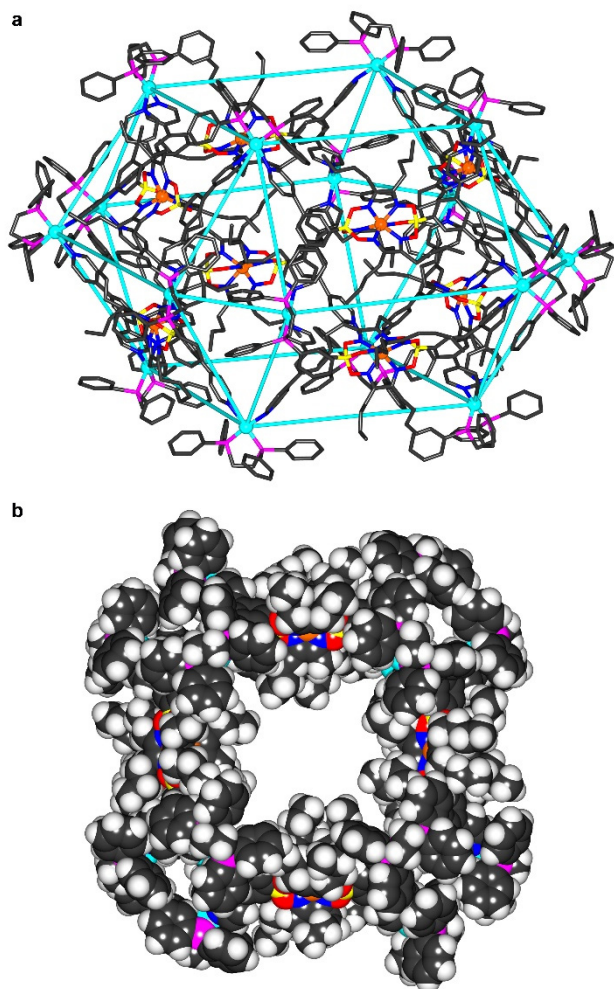


Figure 15. Molecular structure of complex $[(dppe)Pt]_{16}(L11)_8(OTf)_{32}$ in the crystal with view from the side (a) and along the barrel axis (b). The square orthobicupola-like geometry is indicated by (virtual) Pt-Pt bonds. In view b, all atoms are shown with a space-filling representation. Color coding: C: gray, B: yellow, Fe: orange, Pt: cyan, P: purple, N: blue, O: red, H: light gray. Hydrogen atoms (view a) and counter ions are omitted for clarity.

From an enthalpy point of view, the assembly of the $Pt_{2n}L_n$ complexes is controlled by the preferred coordination geometry of the square planar Pt complexes, by the preferred conformation of the rigid metalloligands, and by interactions between the clathrochelate cores of the ligands. Key parameters in this context are the N-Pt-N bond angles, and the distances between Fe atoms of adjacent clathrochelate complexes in the assembly. Table 2 lists the average values for the seven complexes, which we have been able to characterize crystallographically. It is evident that none of the complexes shows a strained coordination geometry at the Pt centers, with N-Pt-N angles between 81 and 88°. Similar values are found for adducts of C1–C4 with other pyridine ligands.¹⁷ As predicted theoretically (Figure 5), the Fe centers of adjacent clathrochelate complexes are further apart from each other in gyrobifastigium-like structures when com-

pared to tetragonal barrel structures. Not surprisingly, the largest average Fe...Fe distance is found for the square orthobicupola. However, this assembly is disfavored from an entropic point of view, and therefore only formed in small amounts.

Table 2. Average N–Pt–N angles (°) and Fe...Fe distances (Å) as determined by X-ray crystallography.^a

ligand	complex	assembly	N–Pt–N	Fe...Fe
L9	C2	tetragonal barrel	81.60	9.125
L12	C1	tetragonal barrel	86.16	9.921
L9	C4	gyrobifastigium	84.86	11.672
L10	C4	gyrobifastigium	83.87	11.982
L11	C4	gyrobifastigium	82.18	11.939
L10	C1	pentagonal barrel	80.89	10.147
L11	C3	orthobicupola	87.90	15.646

^a The average Fe...Fe distance was calculated for all metalloligands, which are directly connected by at least one Pt complex.

From the data presented above, it can be concluded that Pt_3L_4 complexes are the preferred products for reactions between the metalloligands L9–L12 and the *cis*-blocked Pt^{II} complexes C1–C4. Smaller Pt_6L_3 complexes, as observed for other tetratopic pyridyl ligands,³ were not observed, presumably because of steric interactions between the bulky clathrochelate cores of the ligands. Steric interactions between the central parts of the ligands are also the likely cause for the preferred formation of gyrobifastigium-like structures for several L/C combinations. However, the energetic difference between gyrobifastigium- and alternative structures (e.g. tetragonal or pentagonal barrels) is apparently not large, and mixtures of products were thus observed for several L/C combinations. In the following section, we show how it is possible to direct the assembly process towards a defined reaction product, namely pentagonal $Pt_{10}L_5$ barrels.

Pentagonal barrels based on dinuclear metalloligands:

One conclusion of our geometrical analysis was that gyrobifastigium-like structures can only form for tetratopic ligands with a certain aspect ratio (as defined by the distances of the N-donor atoms). Increasing the length of ligands, while keeping the shorter N...N distance constant, should lead to an unfavorable situation for a gyrobifastigium-like structure (Figure 6). This analysis prompted us to explore the utilization of metalloligands based on dinuclear clathrochelate complexes. Similar to their mononuclear counterparts, dinuclear clathrochelate complexes can be prepared by metal-templated condensation reactions involving boronic acids.¹⁸ It is possible to introduce functional groups in apical position by using the corresponding boronic acid.¹⁹ The tetratopic metalloligands L13 and L14 (Figure 16, a) were prepared by four-fold cross-coupling reaction of a Zn-clathrochelate complex with terminal 3,5-dibromophenyl groups with 4-pyridylboronic acid in analogy to a published procedure.²⁰ In addition to the solution-based characterization by NMR spectroscopy and mass spectrometry, we have analyzed the solid state structure of L13 by X-ray crystallography (Figure 16, b and c). The results show that the dinuclear Zn complex is approximately 3 Å longer than the mononuclear Fe complex L9, L11, and L12 (the B...B distances were used for comparison). Furthermore, it is evident that the C₃ symmetric clathrochelate core is sterically very demanding. The higher aspect ratio of the ligands L13 and L14 should disfavor gyrobifastigium-like structures, and the pronounced steric bulk of the

ligands should disfavor both, gyrobifastigium-like structures and tetragonal barrels.

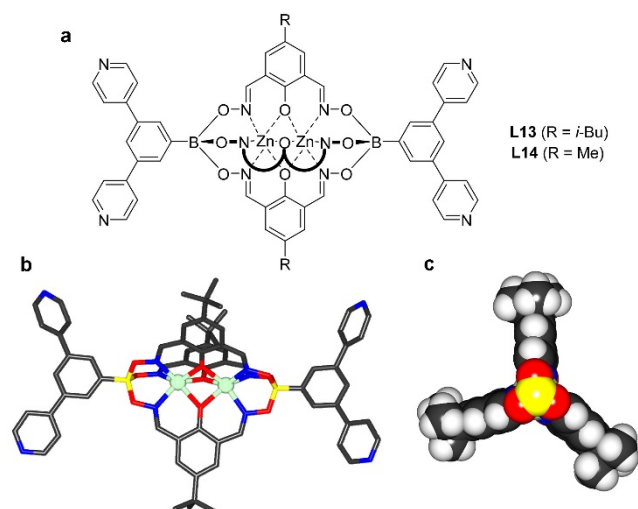
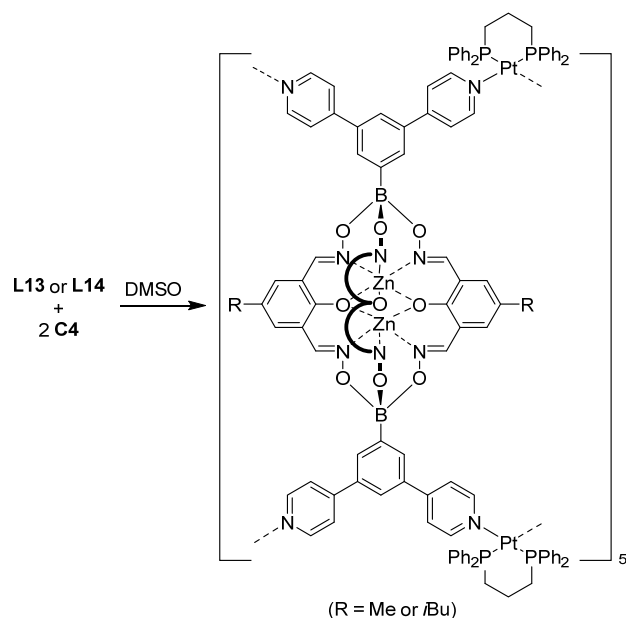


Figure 16. Structures of the metalloligands **L13** and **L14** (a) and the molecular structure of **L13** in the crystal (b and c). For view c, the terminal di(pyridine-4-yl)phenyl groups have been removed to highlight the bulky clathrochelate core. Color coding: C: gray, B: yellow, Zn: light blue, N: blue, O: red, H: light gray.

Subsequently, we have combined the ligands **L13** and **L14** with the platinum complex **C4** (Scheme 2). The reaction was performed in DMSO-*d*₆ (3 d, 50 °C), and the mixture was analyzed by ESI MS and NMR spectroscopy.



Scheme 2. Synthesis of Pentagonal Coordination Barrels.

The analytical data provide strong evidence for the clean formation of pentagonal barrel structures. The mass spectra of the reaction mixtures are rather ‘clean’, and display several strong peaks, which can be assigned to $[(dppp)Pt]_{10}(L13/L14)_5(OTf)_n$ species. The spectrum for the reaction of **L13** and **C4** is shown in Figure 17.

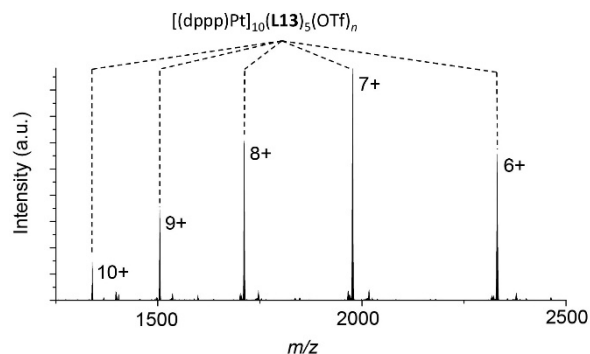


Figure 17. ESI MS spectrum of the reaction between ligand **L13** and complex **C4**.

The ³¹P NMR spectrum of a solution containing **L14** and **C4** shows only one signal, along with the ¹⁹⁵Pt satellites, excluding a gyrobifastigium-like structure or a Pt₁₀L₅ complex of low symmetry (for a model of such a structure see the SI). The NMR spectra of the assembly based on the bulkier ligand **L13** are more complex. Three sets of ¹H NMR signals are observed for the three oximato groups of the clathrochelates. Apparently, there is no free rotation of the clathrochelate cores in the final assembly. Close intramolecular contacts between the clathrochelate complexes in the pentagonal barrel are the likely cause for the reduced rotational freedom. The interdigitating metalloligands render the two phosphorous atoms of the dppp ligand magnetically inequivalent. Accordingly, we observe two doublets in the ³¹P NMR spectrum. Despite numerous attempts, we were unfortunately not able to characterize these pentagonal barrels by X-ray crystallography.

CONCLUSION

The combination of *cis*-blocked, square planar M^{II} complexes with tetra-topic N-donor ligands is known to give supramolecular assemblies of the general formula M_{2n}L_n. We have analyzed different assemblies from a geometrical point of view. This analysis allowed a rationalization of previous experimental results, and it provided guidelines for the targeted synthesis of particular M_{2n}L_n complexes. The theoretical analysis was complemented by extensive experimental studies. Using mononuclear Fe clathrochelate complexes as metalloligands and *cis*-blocked Pt complexes as corners, we have been able to prepare different Pt_{2n}L_n complexes. The outcome of the reactions was found to depend on the nature of the ligand and the Pt complex. Some metal/ligand combinations gave rise to a defined product, whereas mixtures of complexes were observed for others. Importantly, we have identified several metal/ligand combinations, which allow the clean formation of unusual gyrobifastigium structures. By X-ray crystallography, we have been able to characterize new types of M_{2n}L_n complexes, namely a pentagonal Pt₁₀L₅ barrel and a Pt₁₆L₈ complex. The latter assembly is by far the largest structurally characterized M_{2n}L_n assembly described to date, and it displays an unprecedented square orthobicupola geometry. Our theoretical analysis was the foundation for the directed synthesis of pentagonal barrel structures. By combining a *cis*-blocked Pt complex with longer metalloligands, we have been able to prepare such structures in nearly quantitative yields. Overall, we think that our study will provide an important foundation for future investigations of coordination barrels.

ASSOCIATED CONTENT

The Supporting Information is available free of charge on the ACS Publications website at DOI: XXX.

Experimental procedures, analytical data of the ligands and the cages (^1H , ^{13}C , DOSY, HRMS), and further experimental details. (PDF)

X-ray crystallography data: CCDC precursor **9** (1547835), **11** (1547837) and **12** (1547838). Ligands **L9** (1547840), **L11** (1547841), **L12** (1547842) and **L13** (1547844).

Assemblies:

[(dcpe)Pt]₈(**L9**)₄(OTf)₁₆ (1547877)
[(dppp)Pt]₈(**L9**)₄(OTf)₁₆ (1547878)
[(dcpm)Pt]₁₀(**L10**)₅(OTf)₂₀ (1547859)
[(dppp)Pt]₈(**L10**)₄(OTf)₁₆ (1547882)
[(dppe)Pt]₁₆(**L11**)₈(OTf)₃₂ (1547883)
[(dppp)Pt]₈(**L11**)₄(OTf)₁₆ (1547884)
[(dcpm)Pt]₈(**L12**)₄(OTf)₁₆ (1547881)

AUTHOR INFORMATION

Corresponding Author

kay.severin@epfl.ch

Author Contributions

The manuscript was written through contributions of all authors. / All authors have given approval to the final version of the manuscript.

Notes

The authors declare no competing financial interest.

ACKNOWLEDGMENT

The work was supported by the Swiss National Science Foundation and by the Ecole Polytechnique Fédérale de Lausanne (EPFL). We are grateful to the Swiss-Norwegian Beamline Consortium for providing access to synchrotron radiation. We thank Dr. Daniel Ortiz for the MS measurements.

REFERENCES

(1) For selected review articles see: (a) Zarra, S.; Wood, D. M.; Roberts, D. A.; Nitschke, J. R. *Chem. Soc. Rev.* **2015**, *44*, 419. (b) Cook, T. R.; Stang, P. J. *Chem. Rev.* **2015**, *115*, 7001. (c) Lifschitz, A. M.; Rosen, M. S.; McGuirk, C. M.; Mirkin, C. A. *J. Am. Chem. Soc.* **2015**, *137*, 7252. (d) Han, Y.-F.; Jin, G.-X. *Acc. Chem. Res.* **2014**, *47*, 3571. (e) Han, M.; Engelhard, D. M.; Clever, G. H. *Chem. Soc. Rev.* **2014**, *43*, 1848. (f) Agmad, N.; Chughtai, A. H.; Younus, H. A.; Verpoort, F. *Coord. Chem. Rev.* **2014**, *280*, 1. (g) Young, N. J.; Hay, B. P. *Chem. Commun.* **2013**, *49*, 1354. (h) Harris, K.; Fujita, D.; Fujita, M. *Chem. Commun.* **2013**, *49*, 6703. (i) Amouri, H.; Desmarests, C.; Moussa, J. *Chem. Rev.* **2012**, *112*, 2015. (j) Chakrabarty, R.; Mukherjee, P. S.; Stang, P. J. *Chem. Rev.* **2011**, *111*, 6810. (k) Wiester, M. J.; Ulmann, P. A.; Mirkin, C. A. *Angew. Chem. Int. Ed.* **2011**, *50*, 114. (l) Jin, P.; Dalgarno, S. J.; Atwood, J. L. *Coord. Chem. Rev.* **2010**, *254*, 1760. (m) Therrien, B. *Eur. J. Inorg. Chem.* **2009**, 2445. (n) Saalfrank, R. W.; Maid, H.; Scheurer, A. *Angew. Chem. Int. Ed.* **2008**, *47*, 8794. (o) Tranchemontagne, D. J.; Ni, Z.; O'Keeffe, M.; Yaghi, O. M. *Angew. Chem. Int. Ed.* **2008**, *47*, 5136. (p) Dalgarno, S. J.; Power, N. P.; Atwood, J. L. *Coord. Chem. Rev.* **2008**, *252*, 825.

(2) (a) Szalóki, G.; Croué, V.; Allain, M.; Goeb, S.; Sallé, M. *Chem. Commun.* **2016**, 52, 10012. (b) Croué, V.; Goeb, S.; Szalóki, G.; Allain, M.; Sallé, M. *Angew. Chem. Int. Ed.* **2016**, *55*, 1746. (c) Bivaud, S.;

Goeb, S.; Croué, V.; Allain, M.; Pop, F.; Sallé, M. *Beilstein J. Org. Chem.* **2015**, *11*, 966. (d) Bivaud, S.; Goeb, S.; Croué, V.; Dron, P. I.; Allain, M.; Sallé, M. *J. Am. Chem. Soc.* **2013**, *135*, 10018.

(3) (a) Yang, J.; Bhadbhade, M.; Donald, W. A.; Iranmanesh, H.; Moore, E. G.; Yan, H.; Beves, J. E. *Chem. Commun.* **2015**, *51*, 4465. (b) Bivaud, S.; Goeb, S.; Balandier, J.-Y.; Chas, M.; Allain, M.; Sallé, M. *Eur. J. Inorg. Chem.* **2014**, 2440. (c) Bivaud, S.; Balandier, J.-Y.; Chas, M.; Allain, M.; Goeb, S.; Sallé, M. *J. Am. Chem. Soc.* **2012**, *134*, 11968. (d) Bar, A. K.; Mohapatra, S.; Zangrando, E.; Mukherjee, P. S. *Chem. Eur. J.* **2012**, *18*, 9571. (e) Caskey, D. C.; Yamamoto, T.; Addicott, C.; Shoemaker, R. K.; Vacek, J.; Hawkrigge, A. M.; Muddiman, D. C.; Kottas, G. S.; Michel, J.; Stang, P. J. *J. Am. Chem. Soc.* **2008**, *130*, 7620. (f) Yamanoi, Y.; Sakamoto, Y.; Kusukawa, T.; Fujita, M.; Sakamoto, S.; Yamaguchi, K. *J. Am. Chem. Soc.* **2001**, *123*, 980. (g) Fujita, N.; Biradha, K.; Fujita, M.; Sakamoto, S.; Yamaguchi, K. *Angew. Chem. Int. Ed.* **2001**, *40*, 1718.

(4) (a) Bhat, I. A.; Jain, R.; Siddiqui, M. M.; Saini, D. K.; Mukherjee, P. S. *Inorg. Chem.* **2017**, *56*, 5352. (b) Roy, B.; Ghosh, A. K.; Srivastava, S.; D'Silva, P.; Mukherjee, P. S. *J. Am. Chem. Soc.* **2015**, *137*, 11916. (c) Goeb, S.; Bivaud, S.; Croué, V.; Vajpayee, V.; Allain, M.; Sallé, M. *Materials* **2014**, *7*, 611.

(5) Bar, A. K.; Chakrabarty, R.; Mostafa, G.; Mukherjee, P. S. *Angew. Chem. Int. Ed.* **2008**, *47*, 8455.

(6) For other types of coordination barrels see: (a) Yang, L.; He, C.; Liu, X.; Zhang, J.; Sun, H.; Guo, H. *Chem. Eur. J.* **2016**, *22*, 5253. (b) Samanta, D.; Chowdhury, A.; Mukherjee, P. S. *Inorg. Chem.* **2016**, *55*, 1562. (c) Jurček, O.; Bonakdarzadeh, P.; Kalenius, E.; Linnanto, J. M.; Groessel, M.; Knochenmuss, R.; Ihalainen, J. A.; Rissanen, K. *Angew. Chem. Int. Ed.* **2015**, *54*, 15462. (d) Kishi, N.; Akita, M.; Yoshizawa, M. *Angew. Chem. Int. Ed.* **2014**, *53*, 3604. (e) Nakamura, T.; Ube, H.; Miyake, R.; Shionoya, M. *J. Am. Chem. Soc.* **2013**, *135*, 18790. (f) Zarra, S.; Clegg, J. C.; Nitschke, J. R. *Angew. Chem. Int. Ed.* **2013**, *52*, 4837. (g) Riddell, I. A.; Hristova, Y. R.; Clegg, J. K.; Wood, C. S.; Breiner, B.; Nitschke, J. R. *J. Am. Chem. Soc.* **2013**, *135*, 2723. (h) Riddell, I. A.; Smulders, M. M. J.; Clegg, J. K.; Hristova, Y. R.; Breiner, B.; Thoburn, J. D.; Nitschke, J. R. *Nature Chem.* **2012**, *4*, 751. (i) Jung, M.; Kim, H.; Baek, K.; Kim, K. *Angew. Chem. Int. Ed.* **2008**, *47*, 5755. (j) Suzuki, K.; Kawano, M.; Fujita, M. *Angew. Chem. Int. Ed.* **2007**, *46*, 2819.

(7) For examples of tube-like structures see: (a) Howlader, P.; Mukherjee, P. S. *Chem. Sci.* **2016**, *7*, 5893; (b) Meng, W.; League, A. B.; Ronson, T. K.; Clegg, J. K.; Isley, W. C.; Semrouni, D.; Gagliardi, L.; Cramer, C. J.; Nitschke, J. R. *J. Am. Chem. Soc.* **2014**, *136*, 3972. (c) Meng, W.; Clegg, J. K.; Nitschke, J. R. *Angew. Chem. Int. Ed.* **2012**, *51*, 1881. (d) Yamaguchi, T.; Tashiro, S.; Tominaga, M.; Kawano, M.; Ozeki, T.; Fujita, M. *J. Am. Chem. Soc.* **2004**, *126*, 10818. (e) Tashiro, S.; Tominaga, M.; Kusukawa, T.; Kawano, M.; Sakamoto, S.; Yamaguchi, K.; Fujita, M. *Angew. Chem. Int. Ed.* **2003**, *42*, 3267. (f) Su, C.-Y.; Smith, M. D.; zur Loye, H.-C. *Angew. Chem. Int. Ed.* **2003**, *42*, 4085. (g) Aoyagi, M.; Biraha, K.; Fujita, M. *J. Am. Chem. Soc.* **1999**, *121*, 7457.

(8) (a) Kim, Y.; Li, W.; Shin, S.; Lee, M. *Acc. Chem. Res.* **2013**, *46*, 2888. (b) Sakai, N.; Matile, S. *Langmuir* **2013**, *29*, 9031. (c) Sakai, N.; Mareda, J.; Matile, S. *Acc. Chem. Res.* **2008**, *41*, 1354.

(9) Cecot, G.; Alameddine, B.; Prior, S.; De Zorzi, R.; Geremia, S.; Scopelliti, R.; Fadaei, F. T.; Solari, E.; Severin, K. *Chem. Commun.* **2016**, *52*, 11243.

(10) Alvarez, S. *Coord. Chem. Rev.* **2017**, DOI: <http://dx.doi.org/10.1016/j.ccr.2017.03.012>.

(11) For examples of structures with bent alkynyl linkers see: (a) Neuhaus, P.; Cnossen, A.; Gong, J. Q.; Herz, L. M.; Anderson, H. L. *Angew. Chem. Int. Ed.* **2015**, *54*, 7344. (b) Liu, P.; Neuhaus, P.; Kondratuk, D. V.; Balaban, T. S.; Anderson, H. L. *Angew. Chem. Int. Ed.* **2014**, *53*, 7770. (c) Sprafke, J. K.; Odell, B.; Claridge, T. D. W.; Anderson, H. L. *Angew. Chem. Int. Ed.* **2011**, *50*, 5572.

(12) Johannessen, S. C.; Brisbois, R. G.; Fischer, J. P.; Grieco, P. A.; Counterman, A. E.; Clemmer, D. E. *J. Am. Chem. Soc.* **2001**, *123*, 3818.

(13) (a) Jansze, S. M.; Cecot, G.; Wise, M. D.; Zhurov, K. O.; Ronson, T. K.; Castilla, A. M.; Finelli, A.; Pattison, P.; Solari, E.; Scopelliti, R.; Zelinskii, G. E.; Vologzhanina, A. V.; Voloshin, Y. Z.; Nitschke, J. R.; Severin, K. *J. Am. Chem. Soc.* **2016**, *138*, 2046. (b)

Wise, M. D.; Holstein, J. J.; Pattison, P.; Besnard, C.; Solari, E.; Scopelliti, R.; Bricogne, G.; Severin, K. *Chem. Sci.* **2015**, *6*, 1004.

(14) Jansze, S. M.; Wise, M. D.; Vologzhanina, A. V.; Scopelliti, R.; Severin, K. *Chem. Sci.* **2017**, *8*, 1901.

(15) Alvarez, S. *Dalton Trans.* **2005**, 2209.

(16) Zaia, J.; Annan, R. S.; Biemann, K. *Rapid Commun. Mass Spectr.* **1992**, *6*, 32.

(17) Weilandt, T.; Löw, N. L.; Schnakenburg, G.; Daniels, J.; Nieger, M.; Schalley, C. A.; Lützen, A. *Chem. Eur. J.* **2012**, *18*, 16665.

(18) Khanra, S.; Weyhermüller, T.; Bill, E.; Chaudhuri, P. *Inorg. Chem.* **2006**, *45*, 5911.

(19) (a) Marmier, M.; Cecot, G.; Vologzhanina, A. V.; Bila, J. L.; Zivkovic, I.; Rønnow, H. M.; Nafradi, B.; Solari, E.; Pattison, P.;

Scopelliti, R.; Severin, K. *Dalton Trans.* **2016**, *45*, 15507. (b) Marmier, M. D. Wise, J. J. Holstein, P. Pattison, K. Schenk, E. Solari, R. Scopelliti, K. Severin *Inorg. Chem.* **2016**, *55*, 4006. (c) Pascu, M.; Marmier, M.; Schouwey, C.; Scopelliti, R.; Holstein, J. J.; Bricogne, G.; Severin, K. *Chem. Eur. J.* **2014**, *20*, 5592.

(20) Marmier, M.; Cecot, G.; Curchot, B. F.; Pattison, P.; Solari, E.; Scopelliti, R.; Severin, K. *Dalton Trans.* **2016**, *45*, 8422

Graphic for the TOC:

